RESEARCH ON DYNAMIC ACCUMULATION EFFECT AND CONSTITUTIVE MODEL OF ALUMINUM FOAMS UNDER DYNAMIC IMPACT

Hua Gao, Chao Xiong, Junhui Yin, and Huiyong Deng
Army Engineering University, No. 97, Heping West Road, Shijiazhuang 050003, Hebei Province, China

Abstract

Aluminum foams were prepared by melt foaming process. The mechanical properties of aluminum foams under repeated impacts were studied. The porosity and pore size of the prepared aluminum foam were measured. The effects of damage accumulation on the failure morphology of aluminum foam, the transmission rate, stress–strain curve, energy absorption capacity, and the ideal energy absorption efficiency were analyzed. The influence of the number of impacts on the dynamic mechanical properties of the material under the condition of equivalent damage accumulation was studied. Based on the Sherwood–Frost equation, the damage cumulative constitutive model of the aluminum foams under repeated impacts was established. The influence of the difference between the damage cumulative energy corresponding to the reference curve of the shape function and the damage cumulative energy in multiple impacts tests on the prediction accuracy of the constitutive model was analyzed. The results show that with the increase in the number of impacts, the degree of damage to aluminum foam increases, transmission rate increases, the elastic limit stress and the corresponding strain are enhanced, and the damage accumulation effect on aluminum foam under repeated impacts is helpful to improve the ideal energy absorption efficiency. It is verified that the constitutive model can reflect the mechanical properties of aluminum foam under repeated impacts.

Keywords: aluminum foams, dynamic compression, energy absorption efficiency, damage accumulation, constitutive model

Introduction

As a kind of low weight and high specific strength material, aluminum foam material has good capability of resisting explosion buffering and absorbing energy,[1–4] which makes it widely used in military protection, aerospace and other fields, especially for armored protection vehicles. The anti-attack ability is an important index to evaluate its protective performance. Therefore, it is of great value to study the dynamic mechanical properties of aluminum foam materials under repeated impact for scientific research and engineering applications.

Research has been done in the following three aspects at home and abroad: (1) the influence of material parameters and strain rates on the dynamic mechanical behaviors of aluminum foams,[5–7] (2) the deformation process of materials under dynamic load at high temperature,[8–10] (3) the dynamic constitutive model of foam metal materials.[11–13] Kyle et al.[14] analyzed the mechanical behavior of different matrix materials (aluminum, magnesium) and different heat-treated foamed metal materials at high strain rates. The results show that the matrix material and the heat treatment method have a great influence on the compressive properties of materials, and the material exhibits different punching and shearing failure modes under different strain rates. Pengfei[15] analyzed dynamic properties of aluminum foams at high temperature with the help of high-speed photography and found that with the rise in temperature, the strain rate sensitivity of materials is more obvious. While the materials undergo shear fracture at room temperature, the bending failure mode is dominant in high temperature. Using the Hopkinson experiment, Zhang et al.[16] analyzed the dynamic mechanical properties of
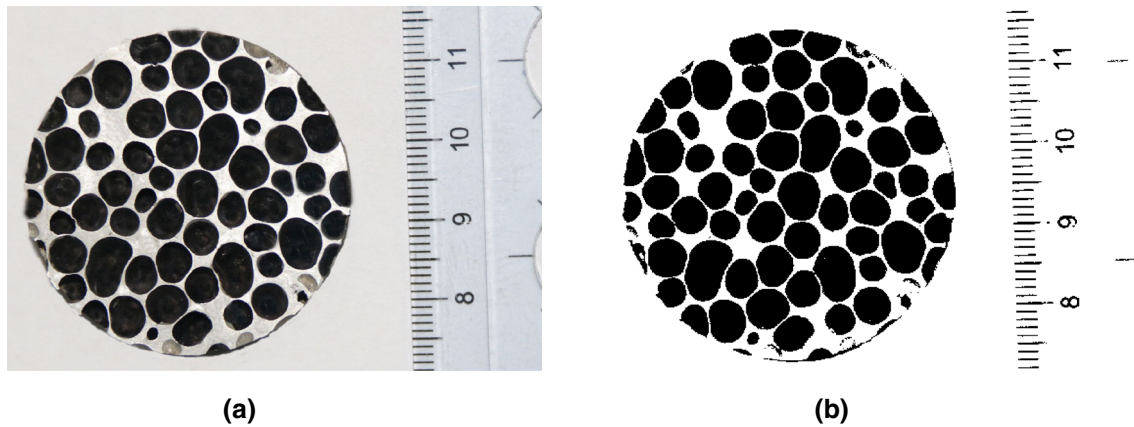
Figure 1. Image of aluminum foams. (a) Initial image of aluminum foams, (b) binary image of aluminum foams.

polyurethane foam aluminum materials including temperature, relative density and strain rate and established the dynamic constitutive model suitable for the relative density and strain rate in a certain range of variation.

All of the above studies are aimed at the dynamic mechanical properties of foam metal under single impact. The damage accumulation caused by multiple impacts is very complicated for the dynamic mechanical properties of materials and so far no systematic study has been done. In this paper, the dynamic mechanical properties of aluminum foams under multiple impacts of low strain rate were investigated using the split Hopkinson pressure bar (SHPB). The variation law of elastic ultimate stress, strain and ideal energy absorption efficiency under different initial impact energies and impact loading times is analyzed, and the damage cumulative variables were introduced to establish the damage cumulative constitutive model under repeated impacts of aluminum foams.

Materials and Experiment

Materials

The aluminum foams were fabricated by adding foaming agent into thickened aluminum melt. The matrix material was pure aluminum (purity > 99.6%), the adjuster for the control of the viscosity of the aluminum melt was pure calcium (purity > 99%), and the foaming agent was hydride zirconium powder (purity > 99%). The aluminum foams were fabricated in the following steps. (1) Melting: pure aluminum was melted in a crucible at 1123 K and cooled to the desired temperature (993–1013 K). (2) Thickening: pure calcium (1.5–3%, mass fraction) was added to the melt at 1123 K and stirred at a constant speed to make its viscosity continuously increased. (3) Mixing: when the viscosity of the melt reached a critical value, the foaming agent (0.6–1.4%, mass fraction) was added to the

melt. At the same time, the mixture was stirred at a higher speed to homogeneously disperse the powder in the whole melt. (4) Holding: the mixture in the furnace was held to decompose the foaming agent. In this stage, bubbles in the melt grew with the holding time until a cellular structure of the melt changed. The structure of the finished product was determined by evolution of bubbles in the foaming melt in this period.

Porosity was the most important microstructural parameter of foam materials, which refers to the available volume fraction of the pores in a finished product. It could be calculated from the mass m and volume V of the sample using the previous expression.[17] Pore size was another important microstructural parameter of this material. The size of each pore in the cross section was determined by software analysis. The sample was dyed black using chemical staining method, and then the cross-sectional surface used for determining the pore size was polished. The pore size could be obtained using image 5.0 after binarization image using MATLAB 7.0. To measure the pore size of aluminum foams, a Canon EOS 70D camera with a resolution of 5472*3648, a focal length of 130.0 mm, an aperture value of F5.6 and a lens model of EF-S18-200mm3.5-5.6IS was used. Under good lighting conditions, the camera is held using a fixture such that the camera's optical axis is perpendicular to the foam aluminum plane. At the same time, a scale is added as a scale reference to obtain a scale factor $\hat{Y}$ indicating the relationship between the distance between the point and the point in the image and the distance between the point and the point in the actual sample (in this paper, $\hat{Y}$ = 10 mm/ 493pixel). The clear image of aluminum foams is obtained by the camera, as shown in Figure 1a. The image is grayed and the binary image is obtained by using the Otsu threshold segmentation method, as shown in Figure 1b. The Canny operator was used for edge detection, and the centroid method was used to obtain the centroid coordinates and the equivalent diameter of the hole. The average
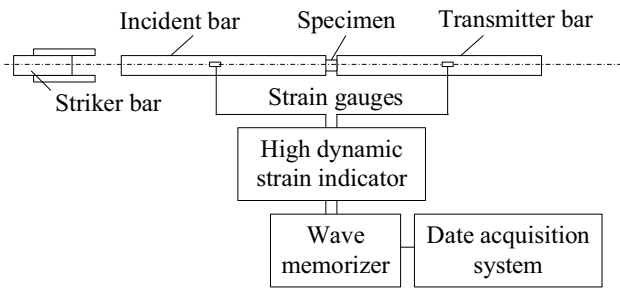
Figure 2. Split Hopkinson pressure bar.

diameter of the hole in the image is calculated to determine the pore size of the sample. The average of the pore size of the five samples was taken as the average pore size of the prepared aluminum foams.

The average pore size is $\bar{D}$. The pore size probability is X_D. The calculation formula for the uniformity is as follows:

$$K = \sum_{0.1\bar{D}}^{1.9\bar{D}} X_D \qquad \text{Eqn. 1}$$

K uniformity; $\sum_{0.1\bar{D}}^{1.9\bar{D}} X_D$ the sum of the pore size probability of pore size in the range of $0.1\bar{D}$–$1.9\bar{D}$.

The test material is a closed-cell aluminum foam with a density of 0.5 g/cm^3 and an average pore diameter of 4 mm. In order to simplify the experimental data processing, aluminum foams are regarded as continuous medium. To obtain effective mechanical properties of the material and reduce the error caused by inertia effect,[18] the sample size is ten times greater than the bubble pore size.[19] Cylindrical test specimens were selected, with a diameter of 40 mm and a thickness of 20 mm. In order to reduce the cell damage of processing in the sample, aluminum foam sample is machined by wire cutting technology.

Experimental Setup

The SHPB test device is mainly composed of a striker, an incident bar and a transmitter bar, as shown in Figure 2.

Aluminum foam is a low-resistance porous material. The impedance of the transmitter bar is so different from that of the sample that the transmitted signal is weak and in the same order of magnitude as the external interference signal, which seriously affects the test result. Therefore, the following improvements are designed: SHPB bar is made of aluminum alloy with small wave impedance, the resistance strain gauges are used on the incident bar and the semiconductor strain gauges with high sensitivity are used on the transmitter bar to record the strain signal. In order to increase the stress wave rising along time to satisfy the internal stress balance of sample, the test process used 8 mm × 8 mm × 3 mm silicone rubber as a waveform shaper. Vaseline is applied at both ends of the aluminum

foam specimen to reduce the deformation friction between specimen and the bar.[20] The diameter of the test pressure bar is 50 mm, and the length of the striker bar, the incident bar and the transmitter bar was 300, 1500 and 1500 mm, respectively.

According to the assumption of uniform stress, the stress–strain curves of aluminum foam samples under different strain rates are obtained by the classical two-wave method as shown in Eqns. 1–4.

$$\sigma(t) = \frac{A}{A_s} E \varepsilon_t(t) \qquad \text{Eqn. 2}$$

$$\dot{\varepsilon}(t) = \frac{2C}{L_s}(\varepsilon_i(t) - \varepsilon_t(t)) \qquad \text{Eqn. 3}$$

$$\varepsilon(t) = \int_0^t \dot{\varepsilon}(t)\,dt \qquad \text{Eqn. 4}$$

where A, C and E are the cross-sectional area of the bar, the wave velocity and the elastic modulus, respectively, L_s and A_s are the thickness and cross-sectional area of samples, $\varepsilon_i(t)$ and $\varepsilon_t(t)$ are strain measured by incident and transmitted signals.

Results and Discussion

On the basis of analyzing the change in material failure topography under repeated impacts by SHPB device, the variation law of the material's wave transmission rate, stress–strain curve and energy absorption efficiency with impact damage accumulation were studied.

Compressive Deformation

In order to analyze the failure process of aluminum foam samples under repeated impacts, five samples were selected to carry out 1 to 5 impact loadings, respectively. The speed of striker bar was 10 m/s. The samples were cut along the loading direction after the impacts. The cross section is shown in Figure 3. After impact, the sample size parameters are shown in Table 1.

As shown in Figure 3, sample 1 was loaded only once, and the cell structure along the loading direction has not been deformed. With the increase in impact, the pore structure is deformed and the phenomenon of collapse compaction occurs.

Stress Wave in Bar

Three samples (A, B and C) were selected. In order to study the effect of initial impact damage on the mechanical properties of aluminum foams under repeated impact, The initial impact energies of A, B and C samples were different in the design of test scheme and the subsequent impact energies were the same. However, due to systematic errors, under the same impact energy, the impact velocity
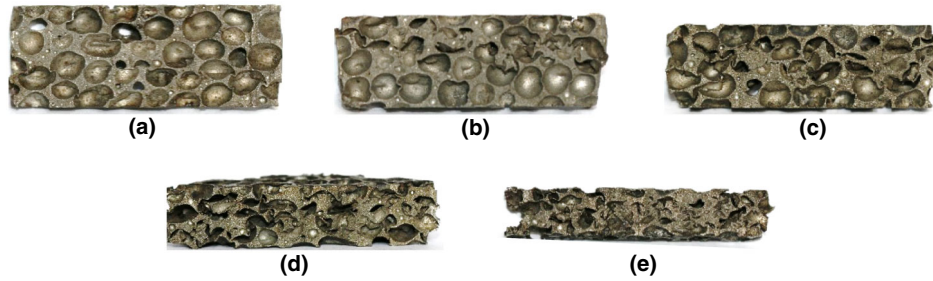
Figure 3. Cross section of specimen after impact loading. (a) Specimen 1 (single impact), (b) specimen 2 (two impact), (c) specimen 3 (three impact), (d) Specimen 4 (four impact), (e) Specimen 5 (five impact).

Table 1. Sample Size Parameters After Impact

Sample number	Diameter (mm)	Thickness (mm)
1	41.40	16.86
2	42.11	13.65
3	43.25	11.19
4	44.67	9.24
5	45.52	7.36

of the striker bar fluctuated in a certain range, as shown in Table 2. A and B were loaded five times. Sample C, due to its high initial impact velocity, produced radial fracture after four loadings and was no longer suitable for impact loading.

Figure 4 shows the incident, reflected and transmitted signals of samples A, B, and C under multiple impacts. Analysis of the wave performance of the samples under repeated impacts is as follows: (1) from the incident waveform, the first incident wave amplitude of sample B, C is higher, and the remaining signal amplitude of other signals is approximately equal; (2) from the reflection waveform, the amplitude of the reflected wave is slightly smaller than that of the incident wave; (3) from the perspective of the transmission waveform, the amplitude of the transmitted wave gradually increases with the increase in impact.

According to the curves of Figure 4, the transmission rate (i.e., the ratio of the peak value of the transmitted wave to the peak value of the incident wave) is calculated to analyze the wave resistance effect of aluminum foams under different impacts. As shown in Figure 5, the sample has a significantly lower rate of transmission rate and a good internal cell structure for initial loading. With the increase in the impact, the damage accumulation increased, the material is compacted, wave resistance performance is reduced, and the wave transmission rate gradually increased.

Dynamic Mechanical Properties

Figure 6 shows the stress–strain curves of aluminum foam samples A, B and C under repeated impacts. As a reference, the static compressive stress–strain curve of aluminum foams is shown in Figure 7. It can be seen that the static and the dynamic mechanical properties of aluminum foams have the same characteristics. The dynamic mechanical properties of aluminum foam can be divided into two stages. In the elastic stage, the aluminum foam is elastically deformed and the stress of aluminum foam increases linearly with strain. In the yield stage, the cell damage strength is reached and the stress will no longer increase. Because of the low impact energy of the striking bar, the characteristics of compaction stage in the high strain rate loading are not found. (As the strain increases, the stress increases rapidly.)

Table 2. Loading Condition of Samples

Sample A	Impact speed (m/s)	Sample B	Impact speed m/s	Sample C	Impact speed (m/s)
A-1	First time 13.6	B-1	First time 17.9	C-1	First time 22.0
A-2	Second time 13.7	B-2	Second time 14.0	C-2	Second time 13.7
A-3	Third time 14.0	B-3	Third time 13.9	C-3	Third time 14.0
A-4	Fourth time 13.8	B-4	Fourth time 13.9	C-4	Fourth time 14.0
A-5	Fifth time 13.8	B-5	Fifth time 14.1		
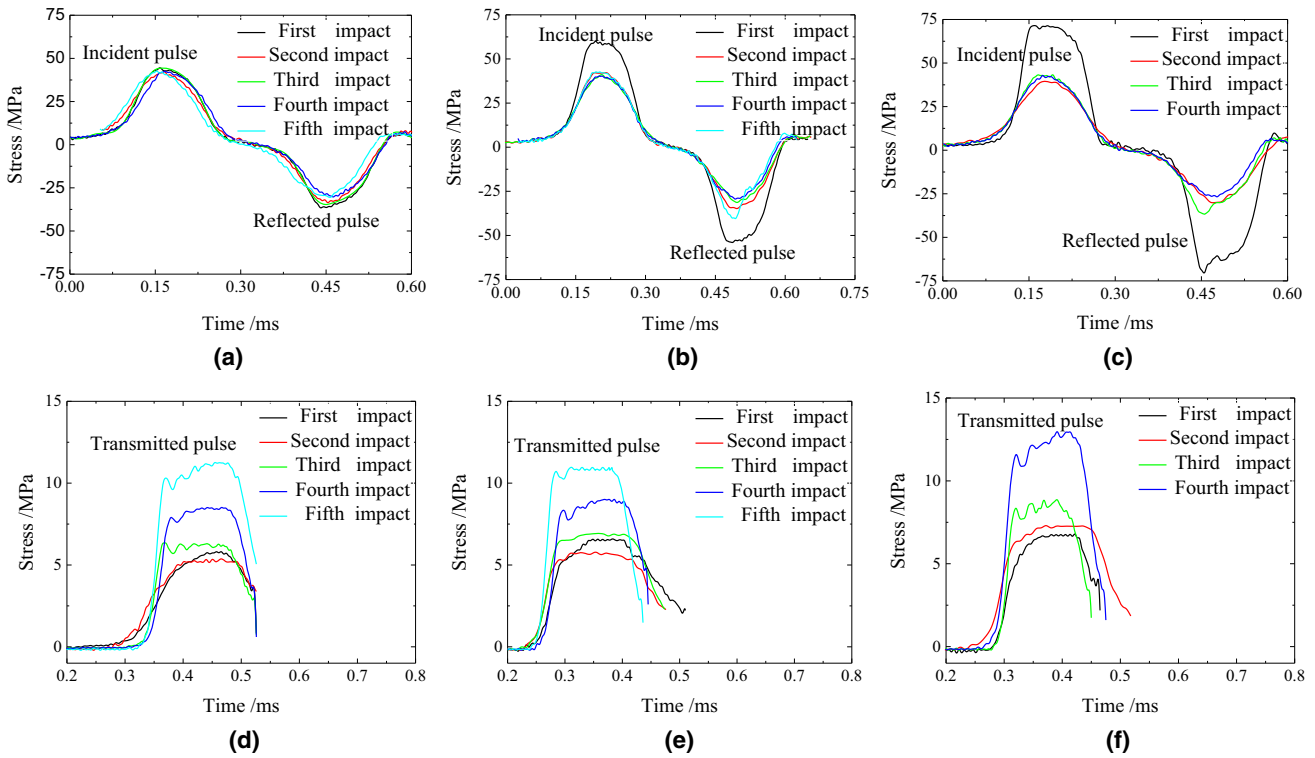
Figure 4. Stress–time relation of incident, reflected and transmitted pulses to specimens under repeated impact. (a) Specimen A, (b) specimen B, (c) specimen C, (d) specimen A, (e) specimen B, (f) specimen C.
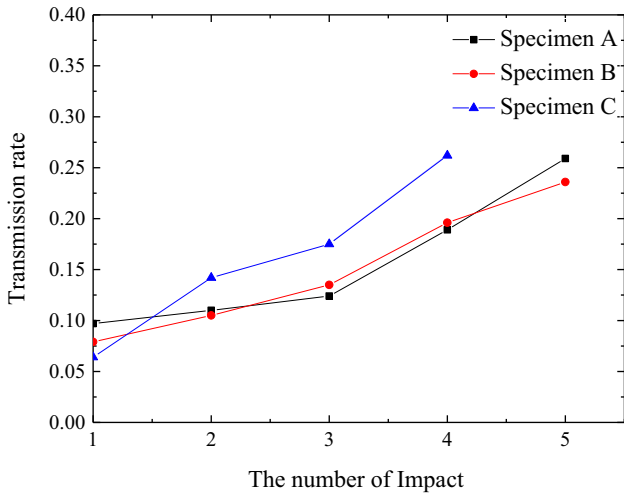

Figure 5. Wave transmitting properties of aluminum foams under.

Comparing the stress–strain curves under repeated impacts, it is found that the yield stage is relatively smooth under the initial loading condition, and the stress amplitude fluctuates with the increase in the number of impacts. The reason is that the initial loading of the cell structure reaches the critical state of yield failure. With the accumulation of damage, cell structure rupture or the degree of fragmentation increases with the unloading, causing the stress to appear.

Figure 8 shows the variation of the elastic ultimate strain of aluminum foam samples A, B, C and the corresponding stress with the number of impacts: (1) For sample A, the initial impact velocity of the striker bar is basically the same as the multiple impact velocity, and the elastic limit strain of the sample increases with the impact frequency. (2) For the specimens B and C, the initial impact velocity of the striker bar is higher than the multiple impact velocity, and the elastic ultimate strain under the initial impact is obviously higher than that under the multiple impacts. The elastic ultimate strain increases with the number of impacts. (3) Under the same impact frequency, the higher the initial impact energy of the samples, the stronger the compaction degree of the cell structure, and the smaller is the corresponding strain of the elastic limit stress. (4) With the increase in the number of impacts, the elastic ultimate stress approximately exponentially increases, showing a significant enhancement effect. The higher the initial load strength of the sample, the higher of the ultimate elastic stress at the same number of impacts.

According to the stress–strain curve of samples A, B, C, impact loading incident energy is calculated by Eqn. 5, as shown in Table 3.

$$W_i = \frac{A_s C_b}{E_b} \int_0^T \sigma_i^2 dt = A_s E_b C_b \int_0^T \varepsilon_i^2 dt \qquad \text{Eqn. 5}$$
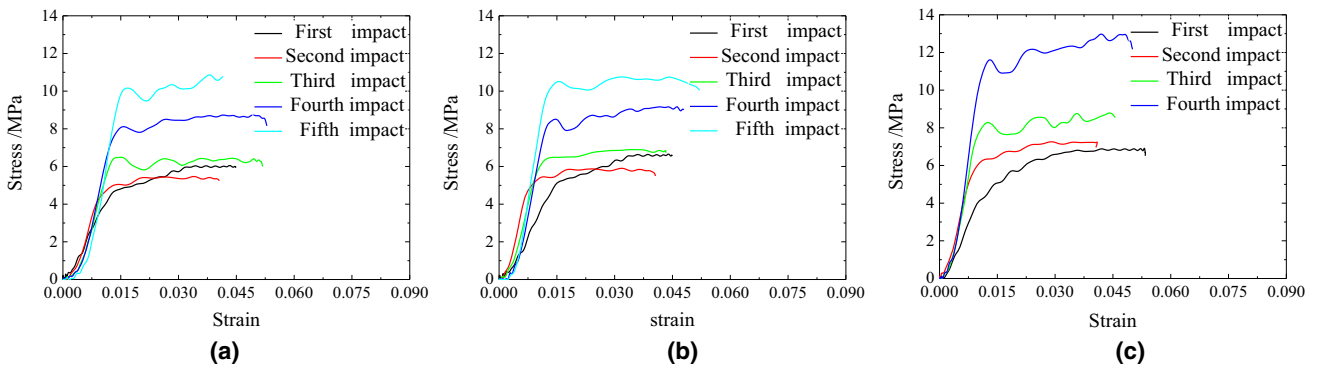
Figure 6. Stress–strain curves of aluminum foams at repeated impacts. (a) Specimen A, (b) specimen B, (c) specimen C.
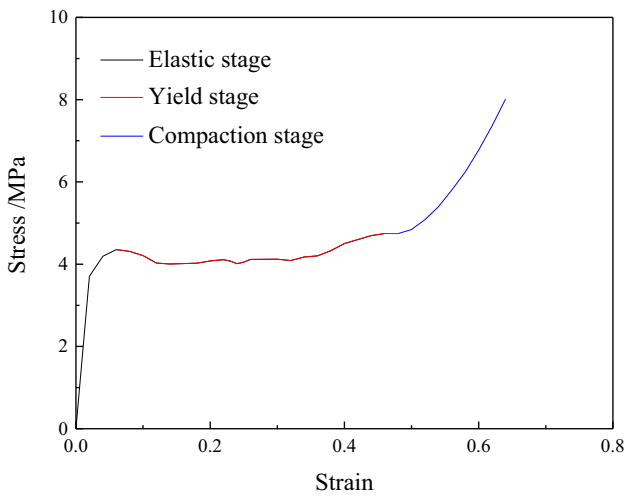

Figure 7. Static compression mechanical properties of aluminum foams.

W_i is the energy of incident wave from the beginning to the unloading; σ_i and ε_i are the incident wave stress and strain; C_b and E_b are the propagation velocity of sound and the elastic modulus of the bar; T is the time from loading to unloading, A_s is the thickness and cross-sectional area of the sample, $\dot{\varepsilon}$ is the strain rate.

It can be seen that A-2 and B-1 have been subjected to two impacts and one impact, respectively, and the damage cumulative energy is 26.73 and 24.23 J; A-3, B-2 and C-1 have been subjected to three, two and one impacts, respectively. The damage cumulative energy is 42.43, 40.42 and 42.3 J, respectively. The stress–strain curves are shown in Figures 9 and 10.

It can be seen from Figures 9 and 10 that the constitutive relations are not the same between the multiple impulses and a complete single impulse (enough energy) under the same damage cumulative energy. The stress of a single sufficient energy impact on the platform segment is obviously higher than that of the platform under multiple
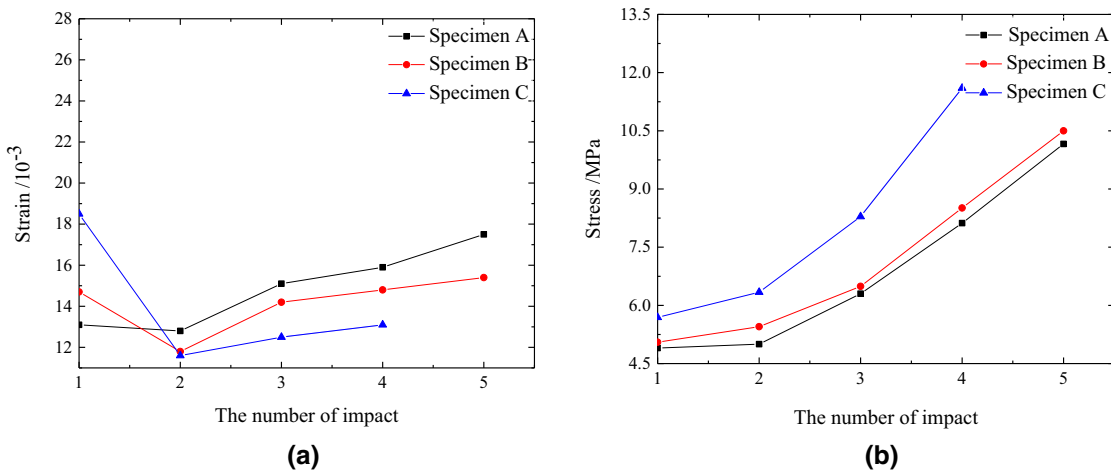

Figure 8. Relation between elastic limit strain, stress and the number of impacts. (a) Elastic limit strain—the number of impacts, (b) elastic limit stress—the number of impacts.

Table 3. Energy Distribution Under Different Impact Loading

Test number	$\dot{\varepsilon}$ (s^{-1})	W_i (J)	Test number	$\dot{\varepsilon}$ (s^{-1})	W_i (J)	Test number	$\dot{\varepsilon}$ (s^{-1})	W_i (J)
A-1	252	12.83	B-1	372	24.23	C-1	438	42.3
A-2	258	13.90	B-2	329	16.19	C-2	343	14.1
A-3	408	15.70	B-3	348	15.1	C-3	496	16.2
A-4	424	14.6	B-4	395	15.3	C-4	444	16.1
A-5	555	14.8	B-5	635	17.2			
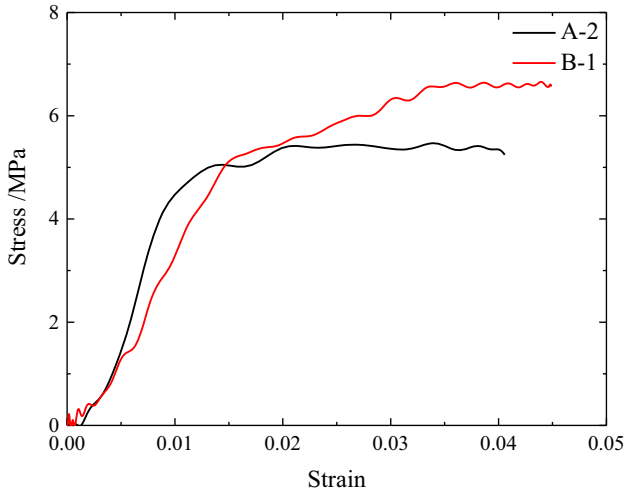
Figure 9. Stress and strain test of A-2 and B-1.
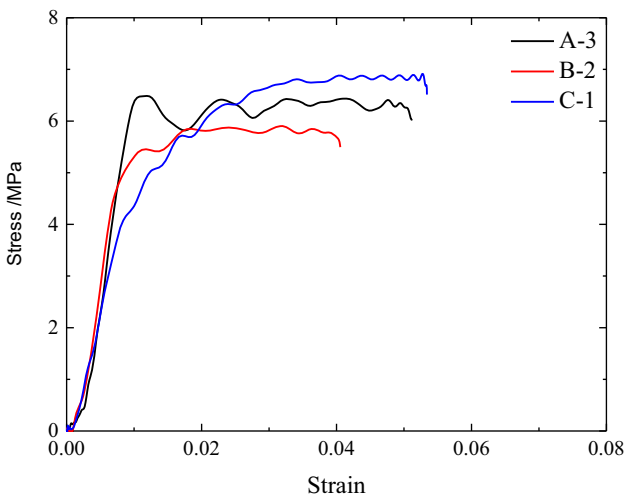
Figure 10. Stress and strain test of A-3, B-2 and C-1.

impacts. With the increase in the number of impacts, the fluctuation of the platform segment increases. This also shows that the damage cumulative effect has a significant effect on the mechanical properties of aluminum foams under repeated impact.

Energy Absorption Analysis

In order to characterize the energy absorption properties of aluminum foams under repeated impacts, the ideal energy absorption efficiency and the energy absorption capacity were analyzed. The ideal energy absorption efficiency η and the energy absorption capacity β can be estimated by References 21 and 22:

$$\eta = \frac{\int_0^\varepsilon \sigma d\varepsilon}{\sigma_{max}\varepsilon} \qquad \text{Eqn. 6}$$

$$\beta = \int_0^\varepsilon \sigma d\varepsilon \qquad \text{Eqn. 7}$$

Here, σ and ε are the optional stress and strain on the compressive stress–strain curve, respectively; and σ_{max} is the maximum stress on the stress–strain curve in the strain range of 0–ε.

Combining the stress–strain curve under the multiple impacts of aluminum foams and the formula of the energy absorption capacity, it can be seen that as the number of impacts increases, the stress platform rises, and the energy absorption capacity of aluminum foams increases.

Figure 11 corresponds to the ideal energy absorption efficiency of aluminum foam samples A, B, C under repeated impacts. The analysis shows that under multiple impacts, as the strain increases, the ideal energy absorption efficiency gradually increases and eventually tends to be smooth. The ideal energy absorption efficiency of the initial impact loading is the lowest in the low-speed loading, the ideal energy absorption efficiency of the second loading is the highest, and then the ideal energy absorption efficiency decreases gradually with the increase in the impact loading frequency. It can be seen that the best ideal energy absorption efficiency of aluminum foams is not in the initial nondestructive state. The cell structure under the condition of yielding or compaction results in damage cumulative effect, and it is more conducive to enhancing the efficiency of aluminum foam energy absorption.
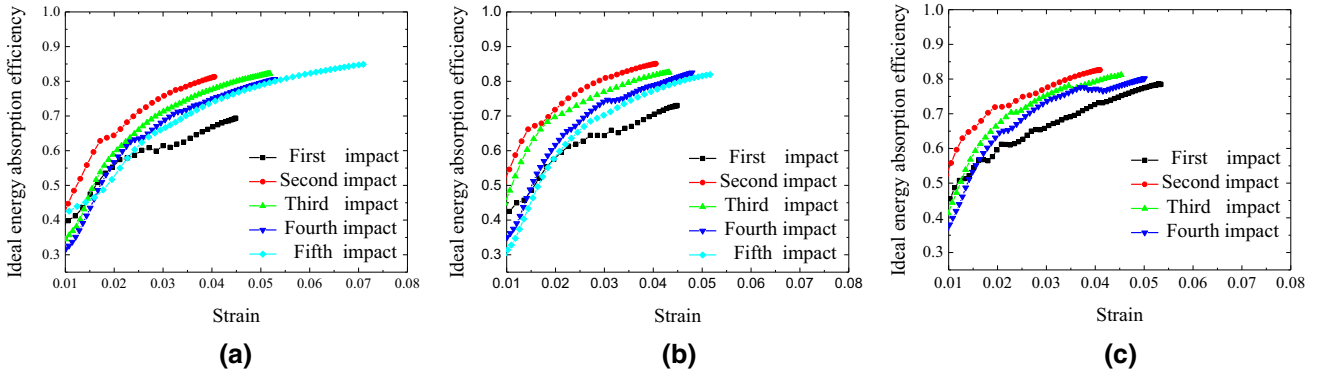
Figure 11. Ideal energy absorption efficiency curves at repeated impacts. (a) Specimen A, (b) specimen B, (c) specimen C.

Table 4. Fitting Parameter of Elastic Limit Stress

m	a_m	b_m	c_m
13.6	0.926	3.279	4.656
17.9	2.861	2.831	5.02
22.0	13.07	2.78	5.93

Damage Cumulative Constitutive Model

Constitutive Model Established

The damage accumulation effect of aluminum foams under multiple impacts makes its dynamic mechanical properties very complicated. Combined with the measured stress–strain curve, based on the Sherwood–Frost equation, the damage cumulative variables are introduced to construct the constitutive model. The common Sherwood–Frost empirical constitutive relation framework for polyurethane foam[23] is:

$$\sigma = H(T_\mathrm{m})G(\rho)M(\varepsilon, \dot{\varepsilon})f(\varepsilon) \qquad \text{Eqn. 8}$$

σ is the stress, T_m is the temperature of the test environment, ρ is the density of the material, ε is the strain, $\dot{\varepsilon}$ is the strain rate, $H(T_\mathrm{m})$ is the temperature influence function, $G(\rho)$ is the density function, $M(\varepsilon, \dot{\varepsilon})$ is the strain rate enhancement; $f(\varepsilon)$ is the shape function.

Sherwood–Frost empirical constitutive relation framework was used for polyurethane foam and was subsequently applied to metal foam.[16,24,25] During the experimental exploration phase, it was found that when the strain rate is too large, a large deformation occurs at the initial impact and multiple impacts cannot be performed. When the strain rate is too small, the degree of cell deformation is very small, and the damage accumulation effect is not obvious. In order to analyze the effect of damage accumulation on the mechanical properties of aluminum foams under multiple impacts, the strain rate range is suitable between 252 and 635 s^{-1}.

Considering the influence of damage variables on the dynamic mechanical properties of materials, the dimensionless damage cumulative variable $\frac{W_m^n}{W_m^1}$ was introduced.

$$\sigma = N\left(\frac{W_m^n}{W_m^1}, \dot{\varepsilon}\right)f(\varepsilon) \qquad \text{Eqn. 9}$$

$$N\left(\frac{W_m^n}{W_m^1}, \dot{\varepsilon}\right) = a_m\left[\ln\left(\frac{W_m^n}{W_m^1}\right)\right]^{b_m} + c_m \qquad \text{Eqn. 10}$$

$N\left(\frac{W_m^n}{W_m^1}, \dot{\varepsilon}\right)$ is the elastic ultimate stress under different initial impact conditions and the number of impacts. W_m^n is the sum of the initial impact to the nth impact incident energy under the condition that the initial impact velocity is m; a_m, b_m, c_m are the corresponding fitting parameters.

From Figure 8b and Table 3, the fitting parameters of the elastic ultimate stress $N\left(\frac{W_m^n}{W_m^1}, \dot{\varepsilon}\right)$ of samples A, B and C can be obtained as shown in Table 4.

It can be seen that the fitting parameters vary greatly with the initial conditions. It is found that a and c are linearly related and quadratic functions with $\frac{W_m^1}{W_{13.6}^1}$, respectively, and b is linear with $\ln\left(\frac{\dot{\varepsilon}_m^1}{\dot{\varepsilon}_{13.6}^1}\right)$. The fitting equations are shown in (11)–(13).

The fitting correlation coefficients of the three curves are 0.998, 0.961 and 0.987, respectively, which has a good fitting effect.

$$a = 2.208\left(\frac{W_m^1}{W_{13.6}^1}\right)^2 - 4.199\frac{W_m^1}{W_{13.6}^1} + 2.917 \qquad \text{Eqn. 11}$$

$$b = -0.9478\ln\left(\frac{\dot{\varepsilon}_m^1}{\dot{\varepsilon}_{13.6}^1}\right) + 3.261 \qquad \text{Eqn. 12}$$

$$c = 0.563\frac{W_m^1}{W_{13.6}^1} + 4.041 \qquad \text{Eqn. 13}$$

Sherwood and Frost[22] express the shape function $f(\varepsilon)$ by the power series, and its expression is

$$f(\varepsilon) = \sum_{p=1}^{q} E_p \varepsilon^p / \sigma_0 \qquad \text{Eqn. 14}$$

Equation of (14) describes the shape of stress–strain curves of aluminum foams under a given reference density, reference initial impact energy and reference damage accumulation. Selecting one stress–strain curve obtained from multiple impacts tests as a reference curve, σ_0 is the elastic ultimate stress corresponding to the reference curve, q is the number of terms expanded by the power series, E_p is the fitting parameter to the reference curve. The stress–strain curve of the above test C-2 as a reference curve and $q = 10$ series was selected to fit the shape function, and the shape function fitting parameters are shown in Table 5.

Thus, the damage cumulative constitutive model of aluminum foams subjected to multiple impacts is shown in Eqn. 15, where a, b, c and $f(\varepsilon)$ are obtained from Eqns. 11–14.

$$\sigma = \left\{ a \left[\ln \left(\frac{W_m^n}{W_m^1} \right) \right]^b + c \right\} f(\varepsilon) \qquad \text{Eqn. 15}$$

In order to verify the constitutive model, multiple impact tests were performed with an initial energy of 35.87 J, an initial strain rate of 397 and followed by three incident energy of 14.1, 15.7, and 15.3 J, respectively. The stress–strain curve obtained from the second, third and fourth impact loadings is compared with the stress–strain curves

obtained from the constitutive model as shown in Figure 12.

The results shown in Figure 12 show that the predictive curve of damage cumulative constitutive model agrees well with the stress–strain curve measured by the test. Compared with the prediction of stress–strain curve of the second and third shocks, discrepancy between the fourth shock prediction curve and the experimental results was more discrete.

The Best Constitutive Model

In order to further determine the influencing factors of the optimal constitutive model, the elastic ultimate stress $N\left(\frac{W_m^n}{W_m^1}, \dot{\varepsilon} \right)$ and the shape function $f(\varepsilon)$ are analyzed.

Figure 13 shows that the constitutive model predicts the elastic ultimate stresses of the second, third and fourth shocks in "Compressive Deformation" section of the test which are 5.99 MPa, 7.88 MPa and 10.33 MPa, respectively. The measured ultimate stress is 6.11 MPa, 8.00 MPa and 10.52 MPa. The errors are 1.9, 1.5 and 1.8%, respectively. It can be seen that the elastic ultimate stress obtained from the constitutive model is in good agreement with the experimental results, and the errors under repeated impacts are not significantly different.

In order to determine the influence of the shape function on the constitutive model, the stress–strain curves of

Table 5. Fitting Parameter of Shape Function

E_1	E_2	E_3	E_4	E_5
-2.9×10^{18}	6.3×10^{17}	-5.8×10^{16}	2.92×10^{15}	-8.8×10^{13}
E_6	E_7	E_8	E_9	E_{10}
1.62×10^{12}	-1.7×10^{10}	8.51×10^7	-9.86×10^4	2.86×10^2
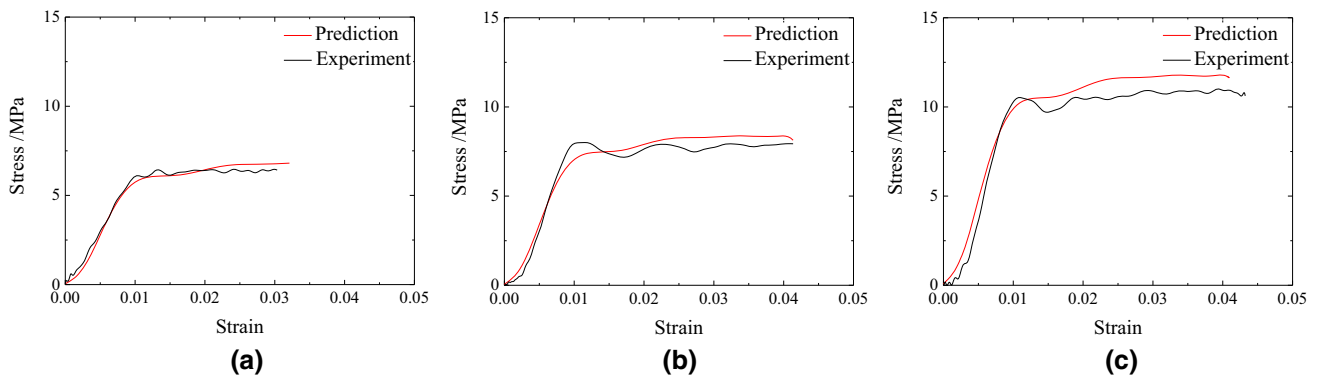
Figure 12. Comparison between calculated and experimental stress–strain curves for aluminum foams. (a) Second impact, (b) third impact, (c) fourth impact.
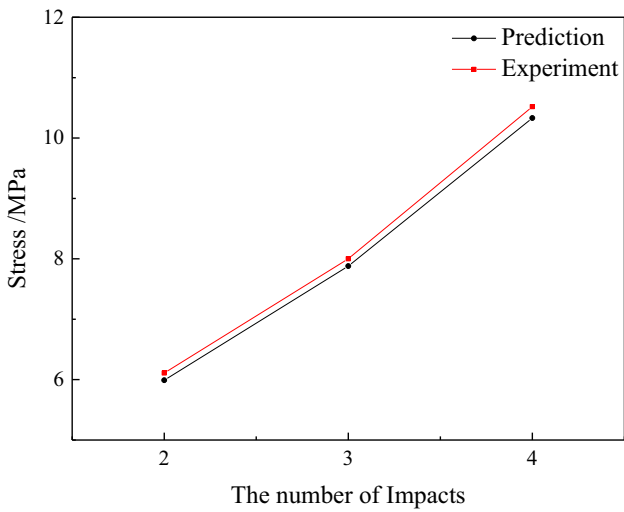
Figure 13. The elastic limit stress predicted by the constitutive and measured by the experiments under repeated impacts.

specimens A, B and C under multiple impacts were selected as the shape function reference curves, respectively, to predict the constitutive relationship of the second, third and fourth shocks in "Compressive Deformation" section. The absolute value of the difference between the damage cumulative energy corresponding to the reference curve of the shape function and the damage cumulative energy in the jth impact is E_j. The discrepancy between the predicted curve and the experimental measured curve is S_j^2. As shown in Eqn. 16

$$S_j^2 = \frac{\sum (\sigma_r - \sigma_e)^2}{v}$$

Eqn. 16

In Eqn. 16, σ_r and σ_e are the predicted stress of the constitutive model and the stress value measured experimentally under the same strain, respectively, and v is the number of experimental acquisition points. Figure 14 shows the difference absolute value of the damage cumulative energy with the J-secondary impact damage cumulative energy for different shape function reference

curves, and the discrete relationship between the predicted curve and the test curve of different shape function reference curves. The analysis shows that the predicted results of the constitutive models with different shape function reference curves have obvious correlation with E_j. Figure 15 shows the distribution of E_j and S_j^2. The larger the absolute value of the difference between the damage cumulative energy of the shape function reference curve and the damage cumulative energy of the test, the greater the discrepancy between the predicted curve of the constitutive model and the experimental curve. This is also evidenced by the positive correlation between the correlation coefficients of E_j and S_j^2 in Figure 15a–c which are 0.91, 0.86 and 0.92, respectively.

The above studies show that the second and third shocks have a good fitting effect because the damage state is similar to that of the experiment C-2. The fourth shock results in a certain error due to the damage accumulation effect. Therefore, selecting the best shape function according to the characteristics of the aluminum foam impact loading test is an important prerequisite for the dynamic mechanical analysis under multiple impacts based on the damage cumulative constitutive model. The smaller the absolute value of the difference between the damage cumulative energy of the shape function reference curve and the damage cumulative energy of the test, the better the predictive effect of the constitutive model is obtained.

Conclusion

The dynamic mechanical properties of aluminum foams were studied under multiple impacts. Based on the experimental results, the damage cumulative constitutive model was constructed. The main conclusions are as follows:

1. With SHPB apparatus, the aluminum foams were subjected to multiple impacts at low and medium strain rates. With the increase in the number of

(a) **(b)** **(c)**
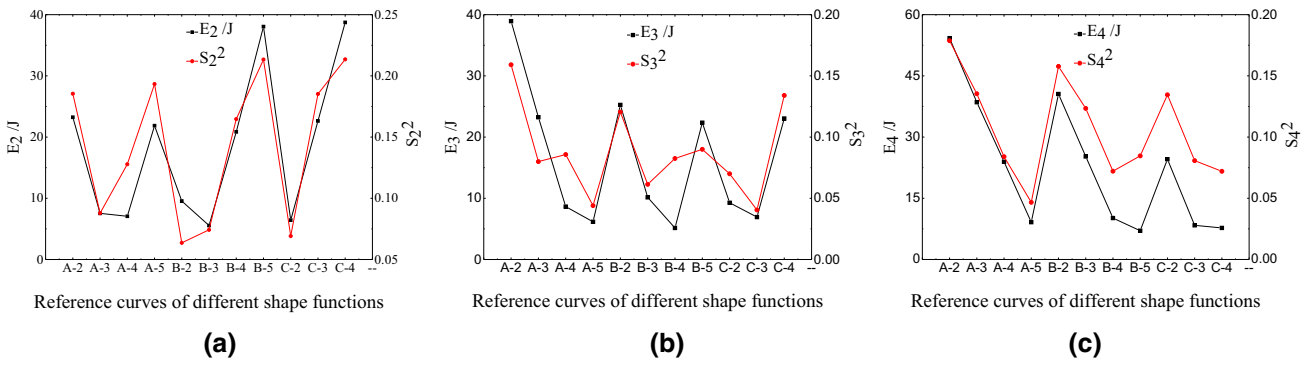
Figure 14. Relationship between reference curves of different shape functions and E_j and S_j^2. (a) Second impact, (b) third impact, (c) fourth impact.
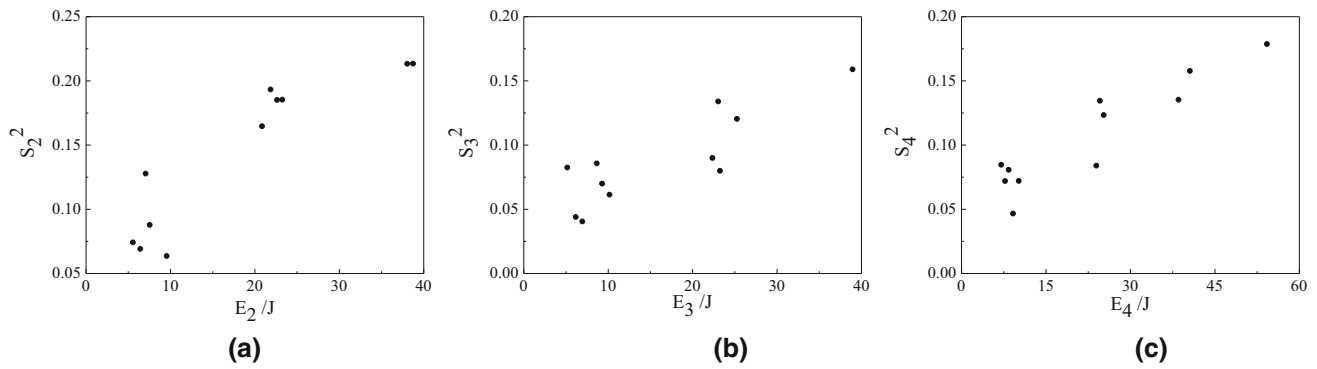
Figure 15. *The relationship between E_j and S_j^2 in three impact test. (a) Second impact, (b) third impact, (c) fourth impact.*

impacts, the cell structure collapsed and compacted gradually, and the attenuating effect of stress waves was weakened.

2. With the increase in the number of impacts, the elastic ultimate strain increases and the elastic ultimate stress grows exponentially, which shows a significant enhancement effect. Under the same impact frequency, the higher the initial impact energy, the higher the corresponding elastic ultimate stress, the lower the corresponding strain of elastic limit stress.

3. The damage accumulation under the repeated impact of aluminum foams is beneficial to improve the energy absorption efficiency and make the constitutive model more complicated. Based on the stress–strain curves combined with the experiment, the damage cumulative variables are introduced into the Sherwood–Frost equation and the damage cumulative constitutive model of aluminum foams under repeated impact was established. The smaller the absolute value of the difference between the damage cumulative energy of the shape function reference curve and the damage cumulative energy of the test, the better the predictive effect of the constitutive model is obtained.

List of symbols

$\bar{D}$	Average pore size
X_D	Pore size probability
K	Uniformity
A	Cross-sectional area of the bar
C	Wave velocity
E	Elastic modulus
L_s	Thickness of samples
A_s	Cross-sectional area of samples
$\varepsilon_i(t)$	Strain on the incident bar
$\varepsilon_t(t)$	Strain on the transmitted bar
W_i	Energy of incident wave from the beginning to the unloading
σ_i	Incident wave stress
T	The time from loading to unloading
$\dot{\varepsilon}$	Strain rate
$\sigma_{\max}$	Maximum stress on the stress–strain curve in the strain range of 0–ε
η	Ideal energy absorption efficiency
T_m	Temperature of the test environment
ρ	Density of the material
$H(T_m)$	Temperature influence function
$G(\rho)$	Density function
$M(\varepsilon, \dot{\varepsilon})$	The strain rate enhancement
$f(\varepsilon)$	Shape function
$N(W, \dot{\varepsilon})$	Elastic ultimate stress under different initial impact conditions
W_m^n	The sum of the initial impact to the nth impact incident energy under the condition that the initial impact velocity is m
a_m, b_m, c_m	The corresponding fitting parameters
σ_0	The elastic ultimate stress corresponding to the reference curve
q	The number of terms expanded by the power series
E_p	The fitting parameter to the reference curve
E_j	The absolute value of the difference between the damage cumulative energy corresponding to the reference curve of the shape function and the damage cumulative energy in the jth impact
S_j^2	The discrepancy between the predicted curve and the experimental measured curve

REFERENCES

1. F. Binesh, J. Zamani, M. Ghiasvand, Ordered structure composite metal foams produced by casting. Int. J. Metalcast. **12**, 89–96 (2018)

2. M. Goel, V. Matsagar, A. Gupta, Blast resistance of stiffened sandwich panels with aluminum cenosphere syntactic foam. Int. J. Impact Eng **77**, 134–146 (2015)

3. M. Alizadeh, M. Mirzaei-Aliabadi, Compressive properties and energy absorption behavior of Al–Al$_2$O$_3$ composite foam synthesized by space-holder technique. Mater. Des. **B35**, 419–424 (2012)

4. I. Orbulov, Compressive properties of aluminum matrix syntactic foams. Mater. Sci. Eng., A **555**, 52–56 (2012)

5. Y. Wang, C. Wang, Effect of structure characteristic parameters and strain rate on the compressive mechanical properties of aluminum foams. Acta Armamentarii **32**, 106–111 (2011)

6. W. Xie, H. Du, S. Li, Experimental study on dynamic mechanical performance of polyurethane-aluminum foams composites. Acta Mater. Compos. Sin. **28**, 103–108 (2011)

7. Y. Alvandi-Tabrizi, D. Whisler, H. Kim, A. Rabiei, High strain rate behavior of composite metal foams. Mater. Sci. Eng., A **631**, 248–257 (2015)

8. P. Wang, S. XU, S. HU, Compressive behavior and deformation mechanism of aluminum foam under different temperature. J. Vib. Shock **32**, 16–19 (2013)

9. C. Cady, G. GrayIII, C. Liu, Compressive properties of a closed-cell aluminum foam as a function of strain rate and temperature. Mater. Sci. Eng., A **525**, 1–6 (2009)

10. M.S. Aly, Behavior of closed cell aluminum foams upon compressive testing at elevated temperatures: experimental results. Mater. Lett. **61**, 3138–3141 (2007)

11. Y. Zhang, G. Sun, X. Xu, Identification of material parameters for aluminum foam at high strain rate. Comput. Mater. Sci. **74**, 65–74 (2013)

12. Y. Ding, L. Yang, L. Wang, Experimental determination of dynamic constitutive parameters for aluminum foams. Explos. Shock Waves **35**, 1–8 (2015)

13. J. Harrigan, S. Reid, P. Tan, High rate crushing of wood along the grain. Int. J. Mech. Sci. **47**, 521–544 (2005)

14. M. Kyle, K. Balint, C. Pedro, Quasi-static and high strain rate response of aluminum matrix syntactic foams under compression. Compos. A **79**, 82–91 (2015)

15. P. Wang, S. Xu, Z. Li, Temperature effects on the mechanical behavior of aluminum foam under dynamic loading. Mater. Sci. Eng., A **599**, 174–179 (2014)

16. Y. Zhang, L. Chen, R. Chen, Dynamic mechanical property experiment and constitutive model establishment of polyurethane foam aluminum. Explos. Shock Waves **34**, 373–378 (2014)

17. L.B. Matijasevic, J. Banhart, S. Fiechter, O. Gorke, Modification of titanium hydride for improved aluminum foam manufacture. Acta Mater. **54**, 1887–1900 (2006)

18. L. Bertholf, C. Karnes, Two-dimensional analysis of the SHPB system. J. Mech. Phys. Solids **23**, 1–19 (1975)

19. Z. Wang, X. Cao, H. Ma, Experimental studies on the dynamic compressive properties of open-celled aluminum alloy foams. Explos. Shock Waves **26**, 46–52 (2006)

20. R. Hartley, T. Cloete, G. Nurick, An experimental assessment of friction effects in the spilt Hopkinson pressure bar using the ring compression test. Int. J. Impact Eng **34**, 1705–1728 (2007)

21. B. Zhang, Y. Lin, S. Li, Quasi-static and high strain rates compressive behavior of aluminum matrix syntactic foams. Compos. B **98**, 288–296 (2016)

22. H. Yu, Z. Guo, B. Li, G. Yao, H. Luo, Y. Liu, Research into the effect of cell diameter of aluminum foam on its compressive and energy absorption properties. Mater. Sci. Eng., A **32**, 454–455 (2007)

23. J. Sherwood, C. Frost, Constitutive modeling and simulation of energy absorbing polyurethane foam under impact loading. Polym. Eng. Sci. **32**, 1138–1146 (1992)

24. Y. Hu, C. Wang, S. Hu, An empirical dynamic constitutive model for aluminum foams and its implementation in LS-DYNA. Acta Armamentarh **35**, 46–50 (2014)

25. Z. Wang, L. Jing, L. Zhao, Elasto-plastic constitutive model of aluminum alloy foam subjected to impact loading. Trans. Nonferr. Metals Soc. China **21**, 449–454 (2011)